

# Improved Nearest Neighbor Methods for Gamma Photon Interaction Position Determination in Monolithic Scintillator PET Detectors

Herman T. van Dam, Stefan Seifert, Ruud Vinke, Peter Dendooven, Herbert Löhner, Freek J. Beekman, and Dennis R. Schaart

**Abstract**—Monolithic scintillator detectors have been shown to provide good performance and to have various practical advantages for use in PET systems. Excellent results for the gamma photon interaction position determination in these detectors have been obtained by means of the  $k$ -nearest neighbor ( $k$ -NN) method. However, the practical use of monolithic scintillator detectors and the  $k$ -NN method is hampered by the extensive calibration measurements and the long computation times. Therefore, several modified  $k$ -NN methods are investigated that facilitate as well as accelerate the calibration procedure, make the estimation algorithm more efficient, and reduce the number of reference events needed to obtain a given lateral ( $x, y$ )-resolution. These improved methods utilize the information contained in the calibration data more effectively. The alternative approaches were tested on a dataset measured with a SiPM-array-based monolithic LYSO detector. It appears that, depending on the number of reference events,  $\sim 10\%$  to  $\sim 25\%$  better spatial resolution can be obtained compared to the standard approach. Moreover, the methods amongst these that are equivalent to calibrating with a line source may allow for much faster and easier collection of the reference data. Finally, some of the improved methods yield essentially the same spatial resolution as the standard method using  $\sim 200$  times less reference data, greatly reducing the time needed for both calibration and interaction position computation. Thus, using the improvements proposed in this work, the high spatial resolution obtainable with the  $k$ -NN method may come within practical reach and, furthermore, the calibration may no longer be a limiting factor for the application of monolithic scintillator detectors in PET scanners.

**Index Terms**—Calibration, entry point, line source, monolithic scintillator detector, nearest neighbor method, position of interaction.

## I. INTRODUCTION

MONOLITHIC scintillation crystals read out by position sensitive photosensors are investigated as alternatives to detectors based on segmented crystals in positron emission tomography (PET) [1]–[7]. These monolithic scintillator detectors have several favorable characteristics, especially for full body

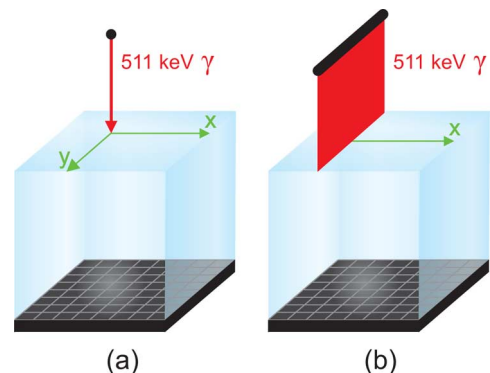


Fig. 1. (a) Illustration of a monolithic scintillator detector irradiated at a given position ( $x, y$ ) by a perpendicularly incident beam of gamma photons. (b) The same detector irradiated along a line parallel to the  $y$ -axis at a given  $x$ -coordinate.

clinical PET systems. They exhibit excellent depth-of-interaction (DOI) correction as well as good spatial resolution, and, since they allow for reduced dead space, high system sensitivity can be obtained [6], [8]. Furthermore, they have several practical advantages, such as easier detector assembly.

The determination of the interaction position of a gamma photon in a monolithic scintillator is more complex than in a detector based on segmented crystals in which the lateral interaction coordinates ( $x, y$ -plane, see Fig. 1(a)) are usually determined by crystal segment identification. For example, in a monolithic scintillator detector the position of the sensor pixel with the largest signal does not necessarily correspond to the ( $x, y$ )-coordinates of the interaction position, since a large fraction of the scintillation photons may be reflected one or more times within the crystal before being detected. Furthermore, the scintillation photons typically spread over many sensor pixels, increasing the relative statistical variance on the number of detected photons per pixel and increasing the influence of electronic noise.

In previous works we determined the entry points of annihilation photons on the crystal front surface using the  $k$ -nearest neighbor ( $k$ -NN) method [6], [9]. It was shown that this approach offers excellent spatial resolution while the influence of parallax errors on the calculated line-of-response (LOR) is kept very small. However, the calibration of the detector is cumbersome as it requires the acquisition of a large set of reference data by irradiating the crystal with a thin beam of annihilation

Manuscript received December 06, 2010; revised March 04, 2011; accepted April 12, 2011. This work was supported by SenterNovem Grant IS055019.

H. T. van Dam, S. Seifert, F. J. Beekman, and D. R. Schaart are with the Delft University of Technology, 2629 JB Delft, The Netherlands (e-mail: d.r.schaart@tudelft.nl).

R. Vinke, P. Dendooven, and H. Löhner are with the KVI, University of Groningen, 9747 AA Groningen, The Netherlands.

Color versions of one or more of the figures in this paper are available online at <http://ieeexplore.ieee.org>.

Digital Object Identifier 10.1109/TNS.2011.2150762

photons at a large number of known entry points and at many different angles of incidence.

To illustrate this issue, one could do the following crude extrapolation. Suppose one would use the measurement setup described in Section V of this work, without any further optimization. In that case, due to the relatively low source activity and the high degree of collimation of the calibration beam, the count rate during calibration would be less than 10 counts per second. The corresponding time to calibrate a single detector of several square centimeters at a few thousand entry points and at a few hundred angles of incidence would be in the order of years.

Furthermore, entry point estimation with the standard  $k$ -NN method is computationally expensive, since the measured light distribution of an event under test has to be compared to those of a large number of reference events.

Again for illustration, an exemplary computation time in the order of  $\sim 0.1$  s per event might be assumed for a basic, non-optimized implementation of the  $k$ -NN algorithm on a single CPU. At this rate, the computation time for calculating the positions of interaction for a typical clinical PET scan of several hundreds of millions of coincidences would be in the order of years.

Clearly, the practical advantages of monolithic scintillator detectors and the high spatial resolution achievable with the  $k$ -NN method may only come within reach for practical use in PET scanners if the calibration procedure can be simplified, the estimation algorithms can be made more efficient, and the number of required reference events can be reduced.

In this work we investigate and compare several possible modifications of the standard  $k$ -NN method that can be used to fulfill these objectives. Various enhancements of the  $k$ -NN method reduce the number of reference events needed to obtain a given  $(x, y)$ -resolution, accelerating both calibration and computation. These modified algorithms utilize the information contained in the calibration data more effectively. Additionally, several of the modified  $k$ -NN methods enable the use of calibration data obtained with a line source, allowing for much easier and faster calibration.

Each of the improved approaches, as well as combinations thereof, are tested on a dataset measured with a SiPM-based monolithic LYSO detector, by evaluating the spatial resolution as well as the bias sensitivity of the modified estimation methods as a function of irradiation position and amount of reference data. The results are compared to those obtained with the standard  $k$ -NN method.

## II. IMPROVED DETECTOR CALIBRATION PROCEDURE

The detector calibration can be made much simpler and shorter by using only a perpendicularly incident beam of annihilation photons to collect reference data (see Fig. 1(a)) instead of calibrating at many angles of incidence as required for entry point determination. In the procedure that is followed in this work,  $(x, y)$  interaction coordinates rather than entry points are obtained by means of the  $k$ -NN method. Since this approach requires explicit DOI information, the DOI is to be determined separately by means of another method. It has been shown that this can also be performed using calibration data

obtained with perpendicularly incident gamma photons only, while neither detector modifications nor a priori knowledge of the light transport and/or signal variances are needed [4], [10]. It is emphasized that this approach might decrease the calibration time of a single detector by at least two orders of magnitude, since calibration at several hundred different angles of incidence is no longer necessary.

Further acceleration and facilitation of the calibration procedure could be achieved by irradiating the detector front surface along two series of lines, i.e., one series parallel to the  $x$ -axis and one series parallel to the  $y$ -axis (Fig. 1(b)), instead of at a grid of points (Fig. 1(a)). A line source calibration would require only  $n_{\text{pos},x} + n_{\text{pos},y}$  calibration positions instead of  $n_{\text{pos},x} \times n_{\text{pos},y}$  positions, where  $n_{\text{pos},x}$  and  $n_{\text{pos},y}$  denote the number of calibration positions in the  $x$ - and  $y$ -directions, respectively. Such a procedure could be implemented by either mechanical or electronic collimation. In the first case, one could e.g., use a line source in combination with a slit collimator in between the source and detector. In the second case, one might e.g., place a line source in between the detector under investigation and a coincidence detector equipped with a slit collimator. A line source has the advantages that it can contain a much higher activity, it is easier to produce, and the geometric efficiency for the detection of gamma photons can be much higher. This concept of a line source together with the abovementioned approach of calibrating at a single angle of incidence could potentially reduce the calibration time of a single detector from the order of years to less than an hour. However, this requires a position estimation method that can make use of reference data corresponding to a line of irradiation points instead of singular points.

## III. $K$ -NEAREST NEIGHBOR METHOD (STANDARD METHOD)

The  $k$ -nearest neighbor ( $k$ -NN) method has been introduced by Fix and Hodges [11] and its application for the determination of the entry points of gamma photons in a monolithic scintillator detector has been studied by Maas *et al.* [2]. In the latter work, a calibration measurement is performed in which a reference dataset is collected by perpendicularly irradiating the monolithic scintillator detector with a thin beam of 511 keV photons at a grid of  $n_{\text{pos}}$  known positions (classes). For each irradiation position, the resulting light intensity distributions  $\mathbf{I} = (I_1, I_2, \dots, I_N)$  of  $n_{\text{ref}}$  reference events are recorded, where  $N$  denotes the number of sensor pixels. All of the

$$n_{\text{tot}} = n_{\text{pos}} \cdot n_{\text{ref}} \quad (1)$$

light patterns are normalized such that the sum of all detector signals equals unity. It should be noted that, due to differences in optical coupling, reflector, scintillator response, etc., each detector may in principle require its own reference dataset.

The unknown  $(x, y)$ -coordinates of the annihilation photon interaction position of an event under test (an unclassified event) is subsequently estimated as follows. The Euclidean distance

$$D = \sqrt{\sum_{i=1}^N (I_{\text{test},i} - I_{\text{ref},i})^2} \quad (2)$$

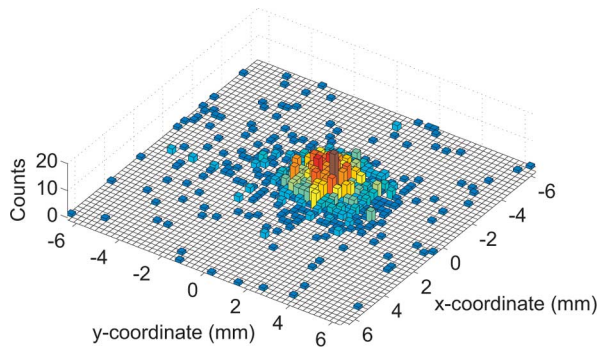


Fig. 2. Example of a NN-histogram. In the standard  $k$ -NN method the most frequently occurring coordinate is assigned to the unclassified event. The improved approaches include e.g., fitting and smoothing the NN-histogram.

of the measured light distribution  $I_{\text{test}}$  to those of all events in the reference set  $I_{\text{ref}}$  is calculated. A subset of the reference data consisting of the  $k$  events with the smallest values of  $D$  (nearest neighbors) is selected and a histogram of their  $(x, y)$  irradiation coordinates is created (see Fig. 2). The coordinate corresponding to the maximum value of the histogram, i.e., the most frequently occurring coordinate, is assigned to the unclassified event. In case of multiple maxima (a tie), one of the maxima is selected randomly. It should be noted that a tie could also be solved by increasing or decreasing  $k$  until a single maximum is obtained [12].

#### IV. IMPROVED NEAREST NEIGHBOR ALGORITHMS

The probability of misclassification approaches the theoretical minimum (i.e., the Bayes error probability) for the standard  $k$ -NN method in the infinite sample case, i.e., if  $k$ ,  $n_{\text{pos}}$ , and  $n_{\text{ref}}$  tend to infinity such that  $k/n_{\text{tot}} \rightarrow 0$  [13]. In practice, however, approaching the conditions for optimal performance of the  $k$ -NN method may be very time consuming. It requires the detector to be irradiated with a large number of annihilation photons at many different known positions. Additionally, the resulting large reference dataset causes the interaction position estimation to be computationally intensive. Moreover, the standard  $k$ -NN method is not guaranteed to be the optimal way of using the information contained in the neighborhood of unclassified patterns in the finite sample case [14].

One reason for this is that the  $k$ -NN method implicitly assumes that the  $k$  nearest neighbors are contained in a relatively small volume. In practice, however, the Euclidean distance  $D$  between the unclassified pattern and one of its closest neighbors is not always negligible. Therefore, it was proposed to give weights to the nearest neighbors based on the distance to the unclassified sample, yielding better results in several cases [15], [16]. Nevertheless, it was shown that the standard  $k$ -NN method still outperforms the weighted method in the infinite sample case [12].

A second reason is that in many cases it cannot be assumed that all classes are represented in the reference dataset, e.g., when the detector irradiation has been performed using a coarse grid. In those cases, an unclassified sample could be far away from any reference sample and most probably belongs to a class for which no reference data has been collected [17].

Yet, another limitation of the  $k$ -NN method is that it offers no obvious way to cope with uncertainty or imprecision in the labeling of the reference data, e.g., due to a finite irradiation beam width or due to Compton scattering in the crystal. Furthermore, even if patterns are correctly labeled, they may be rather atypical for the particular class. Several adapted  $k$ -NN methods based on fuzzy sets theory have been proposed for handling imprecision and uncertainty in a classification process, e.g., by giving less weight to atypical patterns than those that are truly representative of the classes [18].

In literature various alternative NN-approaches have been shown to yield better results than the standard method in the finite sample case in a variety of applications. These approaches include the method proposed by Dudani and Macleod, in which weights are assigned to the nearest neighbors based on their distances to the unclassified sample [15], [16], the different unweighted methods proposed by Bailey and Jain [12], and the kernel based CAP method proposed by Hotta *et al.* [19]. However, these methods appeared to perform similarly to the standard method for the detector investigated in this work and, therefore, they are not discussed further here.

The alternatives to the standard  $k$ -NN method that are presented in this work are based on the fact that all nearest neighbors carry some information. This information can be used more effectively, e.g., by smoothing or fitting the NN-histogram, by means of the so-called categorical average patterns (CAP) method, and/or by combining reference data for each dimension analogous to calibrating with a line source. These methods may be less sensitive to misclassification due to statistical fluctuations in case of small reference datasets and, therefore, they may yield similar results as for large reference datasets, allowing for faster calibration. From all the methods that were tested by means of the cross-validation method described in Section V, only those that appeared to perform best are discussed in the remainder of this work.

##### A. Fit of the $k$ -NN-Histogram (Fit Lorentzian)

In this method the  $k$  nearest neighbors of an unclassified light distribution are selected and a 2D-histogram of their irradiation positions is created (see Fig. 2). So far this is similar to the standard  $k$ -NN method. Now, for sufficiently large reference datasets, we can assume that the irradiation coordinate closest to the true position of interaction has the highest probability of being present in the set of nearest neighbors and that this probability decreases for irradiation coordinates further away from this point. Therefore, all points in the histogram carry some information about the true position of interaction. Using more of this information, instead of only the most frequently occurring coordinate, can reduce statistical fluctuations on the interaction position estimation. Here, this is performed by fitting the histogram with a 2D Lorentzian shaped function using a log-likelihood method. Since the actual shape of the histogram is unknown, several peak shaped functions were tested, of which the Lorentzian shaped function yielded the best results. The coordinate that corresponds to the peak position value of the fit is assigned to the unclassified event. It should be noted that this method allows results in continuous coordinates.

### B. Smoothed $k$ -NN-Histogram (Smoothed)

The 2D irradiation position histogram of the set of  $k$  nearest neighbors is smoothed with a moving average filter of  $n \times n$  bins. Here,  $n = 5$ . Thus, each new bin value is based on the average of 25 bin values of the original histogram. Near the edges of the histogram the number of averaging bins is decreased. The coordinate corresponding to the maximum value of the smoothed histogram is assigned to the unclassified event.

### C. Split 1D $k$ -NN-Histograms (Split 1D Max)

As discussed in Section II, collecting reference data with a line source (see Fig. 1(b)) allows for much easier and faster calibration. If such a line source would be oriented parallel to the  $y$ -direction and scanned along the  $x$ -direction, one would obtain reference line classes, in which each event is assigned to an  $x$ -coordinate only. By following an approach equivalent to the standard  $k$ -NN method, the  $x$ -coordinate of an unclassified event can be determined by comparing its light distribution to all events in these reference line classes. Analogous to the standard  $k$ -NN method, we can assume that the reference line class closest to the true  $x$ -position of interaction has the highest probability of being present in the set of nearest neighbors and that this probability decreases for line classes further away from this point. The  $y$ -coordinate can be obtained similarly by comparing the unclassified event to reference line classes obtained by a scan of a line source along the  $y$ -direction. It should be noted that this approach is enabled by the intrinsic characteristic of the  $k$ -NN method that one has access to all individual reference events.

The procedure is implemented and assessed in the following way. For the determination of the  $x$ -coordinate, a line source oriented parallel to the  $y$ -direction is emulated, where use has been made of the reference data obtained at a grid of points. This is done by combining all reference events corresponding to a given  $x$ -coordinate into a single class. For all events in such a reference line class only the  $x$ -coordinate of each reference event is used. The Euclidean distances  $D$  of the unclassified light distribution to those of all reference events are calculated (see (2)). Then, a 1D-histogram is created of the  $x$ -coordinates of the irradiation positions of the  $k$  nearest neighbors. The coordinate that corresponds to the maximum bin value is the estimated  $x$ -coordinate. The  $y$ -coordinate is then determined in an equivalent way.

### D. Fit of the Split 1D $k$ -NN-Histograms (Split 1D Fit)

This method is equivalent to the previous one, except that the coordinate assigned to the unknown event corresponds to the peak position of a Lorentzian fit of the 1D-histogram.

### E. Categorical Average Patterns (CAP)

The classification scheme of the so-called categorical average patterns (CAP) method makes somewhat different use of the information contained in the reference data than the previous methods [19]. In this method the  $(x, y)$ -position of interaction is estimated by first calculating the Euclidean distances  $D$  of the unclassified light distribution to those of all reference events at a single irradiation position. A subset of these reference events

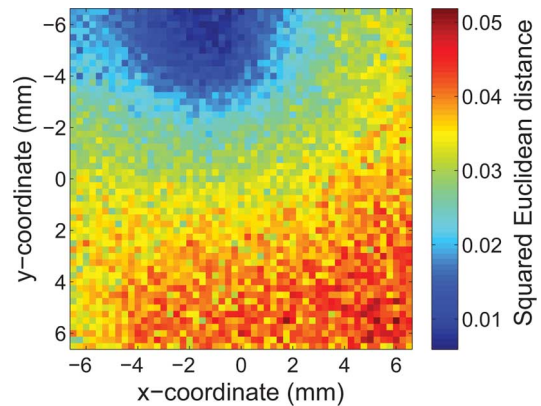


Fig. 3. Illustration of the CAP method showing the squared Euclidean distances of an unclassified light distribution to the average light distributions of the  $k$  nearest neighbors at all irradiation coordinates  $(x, y)$ . In the standard CAP method the coordinate corresponding to the minimum distance is assigned to the unclassified light distribution.

consisting of the  $k_{\text{CAP}}$  nearest neighbors is then selected and an average light distribution is calculated for this subset. This is repeated for each of the  $n_{\text{pos}}$  irradiation positions in the reference dataset. Then, the Euclidean distances of the unclassified light distribution to all of the average light distributions are calculated (see Fig. 3). The coordinate corresponding to the minimum distance is assigned to the unclassified light distribution.

### F. Categorical Average Patterns Smoothed (CAP Smoothed)

This method is equal to the previous one, except that the obtained set of distances of the unclassified light distribution to all of the average light distributions is smoothed with a moving average filter, similar to the filter described in Section IV-B.

### G. Categorical Average Patterns 1D (CAP 1D Min)

In this method the  $x$ - and  $y$ -coordinate are obtained separately. First, only the  $x$ -coordinate of each reference event is used. The Euclidean distances  $D$  of the unclassified light distribution to those of all irradiation positions with one specific  $x$ -coordinate are calculated. A subset of these reference events consisting of the  $k_{\text{CAP}}$  nearest neighbors is then selected and an average light distribution is calculated for this subset. This is repeated for all  $x$ -coordinates of the irradiation positions. Then, the distances of the unclassified light distribution to all average light distributions are calculated. The  $x$ -coordinate corresponding to the minimum distance is assigned to the unclassified light distribution. A similar procedure is used to obtain the  $y$ -coordinate. This method is analogous to collecting reference data with a line source, similarly to the 'split 1D' methods described in Sections IV-C and IV-D.

## V. EXPERIMENTAL METHODS

Measurements were performed with a monolithic scintillator detector based on a  $13.2 \text{ mm} \times 13.2 \text{ mm} \times 10 \text{ mm}$  monolithic  $\text{LYSO}:\text{Ce}^{3+}$  scintillator with optically polished surfaces (Crystal Photonics). A SiPM array (SensL SPMArray 3035G16) is optically coupled to the crystal using Sylgard 527 dielectric gel. All other faces of the crystal are covered with a highly reflective PTFE-based material (Spectralon).

The SiPM array is a  $4 \times 4$  array of SiPM pixels measuring about  $3 \text{ mm} \times 3 \text{ mm}$  each and having a pitch of  $3.3 \text{ mm}$ . Each pixel has an active area of  $2.85 \text{ mm} \times 2.85 \text{ mm}$ , made up of 3640 microcells. The SiPM array was operated at the manufacturer-specified bias voltage of  $29.3 \text{ V}$ , exceeding the nominal breakdown voltage by  $2.0 \text{ V}$  and corresponding to a gain of  $\sim 10^6$ .

The SiPM signals were preamplified using a 16-channel readout board described by Seifert *et al.* [20]. The preamplified SiPM pulses were shaped and their pulse heights digitized using the multichannel data acquisition system described by Maas *et al.* [6].

Reference data were collected by irradiating the detector with perpendicularly incident  $511 \text{ keV}$  gamma photons at a rectangular, equidistant grid of  $(x, y)$ -positions with a pitch of  $0.25 \text{ mm}$  and covering the entire front surface of the crystal. To this end, a Na-22 source was electronically collimated resulting in a beam with a diameter of  $\sim 0.64 \text{ mm}$ . A detailed description of the experiments can be found in [9].

### A. Spatial Resolution

The spatial resolution was determined using a cross-validation method, i.e., the leave-one-out method described by Maas *et al.* [6]. The estimated coordinates are subtracted from the corresponding irradiation coordinates and a 2D-histogram is created, representing the detector spatial response. In this work the  $\sim 0.64 \text{ mm}$  width of the test beam is much smaller than the detector spatial response and, therefore, the histogram approximates the point spread function (PSF) [21]. Since for small sample cases the PSF may suffer from low statistics, the histogram was fitted with an inverse polynomial shaped function

$$f_{\text{fit}} = \frac{p_1}{1 + p_4(p_2x^2 + p_3y^2) + p_5(p_2x^2 + p_3y^2)^2}, \quad (3)$$

where  $p_i$  are fitting parameters. This function has no physical meaning, but it was chosen from a set of tested fitting functions, as it appeared to fit the PSFs best. An average value of the full width at half maximum (FWHM) and the full width at tenth maximum (FWTM) was calculated of the cross sections of the fit in the  $x$ - and  $y$ -directions as well as the two directions with a  $45$  degrees angle to the  $x$ - and  $y$ -direction. This was repeated for different numbers of nearest neighbors and the minimum FWHM and corresponding FWTM were taken as measures of the spatial resolution.

Each interaction position estimation method described in Section IV was tested for different numbers of reference events per irradiation position  $n_{\text{ref}}$  and for different total amounts of reference data  $n_{\text{tot}}$ . This was achieved by subsampling the full reference dataset by randomly removing a given number of events per irradiation position  $n_{\text{ref,remove}}$ . When  $n_{\text{ref,remove}}$  was larger than the remaining  $n_{\text{ref}}$ , the discarded events were used to create an additional equivalent reference dataset with an equal value of  $n_{\text{ref}}$ . In the case that  $n_{\text{tot}}$  was varied both  $n_{\text{ref}}$  and  $n_{\text{pos}}$  were decreased. In this way, the mean value and standard deviation of the spatial resolution were obtained for part of the cases.

The spatial resolution was determined using irradiation coordinates from the entire irradiation grid. Since the spatial reso-

lution appeared to be rather different in the center compared to the edges of the detector, it was also determined for the central  $6.3 \text{ mm} \times 6.3 \text{ mm}$  as well as for the remaining edges of the detector.

### B. Bias Sensitivity

For any algorithm that assigns interaction positions inside a given set of boundaries (e.g., the crystal dimensions), the PSF is truncated and/or asymmetrical near the edges. Systematic measurement errors, such as variations in gain or in offsets, may have a similar effect on the PSF. Such effects are commonly referred to as bias and should be taken into account when modeling the detector spatial response, e.g., for image reconstruction purposes.

Additional bias may arise from the interaction position estimation method itself. In order to compare the relative sensitivity to bias  $S$  of the different methods, the following characterization was performed based on the principle that, if each position is irradiated with  $n_{\text{ref}}$  events, an unbiased method would assign all irradiation positions  $n_{\text{ref}}$  times in the absence of counting statistics.

For each method a 2D-histogram was created of the entire set of estimated interaction positions that were determined using the cross validation method described in IV-A. Subsequently, the number of reference data per irradiation position  $n_{\text{ref}}$  was subtracted from each bin value  $n_{x,y}$ . The result was divided by  $n_{\text{ref}}$ . Then, it was first summed along the  $y$ -direction, the absolute value of each element of the resulting vector was calculated, this vector was summed and, finally, this value was divided by the total number of irradiation positions  $n_{\text{pos}}$ . This results in a relative bias sensitivity

$$S = \frac{\sum_x \left| \sum_y \frac{n_{x,y} - n_{\text{ref}}}{n_{\text{ref}}} \right|}{n_{\text{pos}}}. \quad (4)$$

This procedure was repeated with a reversed order of the two summations. By averaging the resulting two values, a measure for the bias sensitivity was obtained. The bias sensitivity was determined using irradiation coordinates of the entire irradiation grid, the central  $6.3 \text{ mm} \times 6.3 \text{ mm}$ , and the remaining edges of the detector.

## VI. RESULTS AND DISCUSSION

In the remainder of this section the error bars indicate the standard deviations arising from the results of equivalent reference datasets as discussed in Section V-A. It should be noted that for the so-called 1D methods the value of  $n_{\text{ref}}$  corresponds to the number of reference events used for the determination of a single coordinate ( $x$  or  $y$ ).

### A. Spatial Resolution

The spatial resolution calculated as an average over the central part of the detector surface in terms of FWHM and FWTM is shown in Fig. 4(a) and (b), respectively, as a function of  $n_{\text{ref}}$ , where the irradiation grid spacing was kept constant at  $0.25 \text{ mm}$ . Fig. 5(a) and (b) show the same for the detector edges. In all cases all alternative methods outperform the standard method.

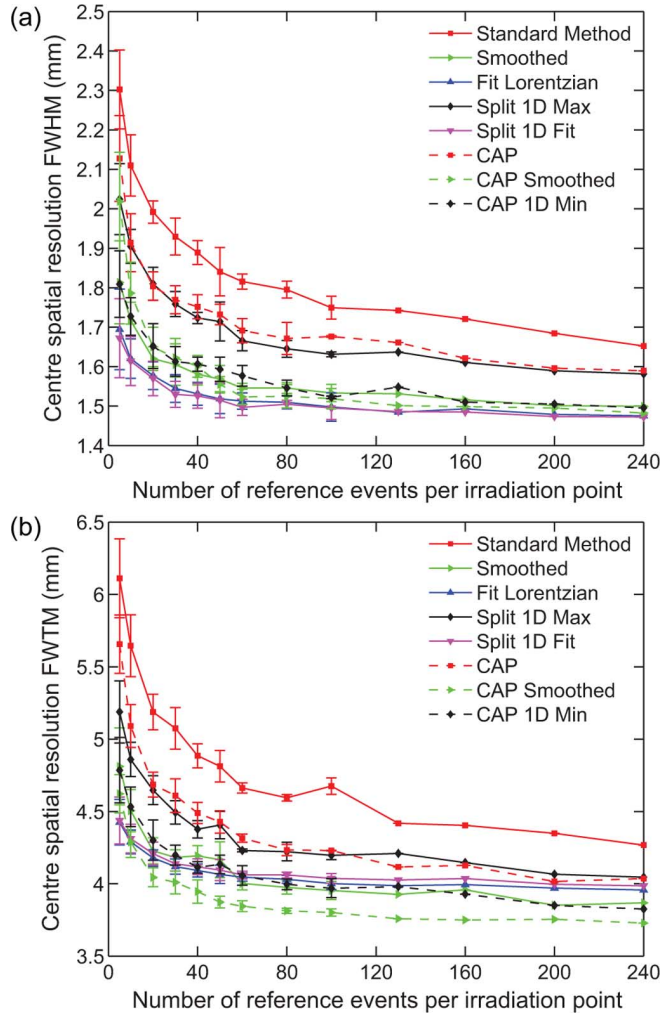


Fig. 4. Spatial resolution in terms of (a) FWHM and (b) FWTM calculated as an average over the central part of the detector surface as a function of  $n_{ref}$  for all methods investigated using a constant irradiation grid spacing of 0.25 mm.

The five best performing methods yield approximately equal results, i.e.,  $\sim 1.5$  mm in terms of FWHM, at high  $n_{ref}$  in the central part of the detector.

For all methods, the spatial resolution is better in the center of the detector than at the edges, both in terms of FWHM and FWTM. This is in agreement with previous findings [2], [6]. It suggests that the spatial resolution may be substantially improved by enlarging the detector area, resulting in a relatively large central area. Here, it should be noted that this improvement might be limited by a possible increase of statistical fluctuations on the number of detected photons per pixel and/or by electronic noise. Furthermore, a larger detector area might result in increased dead time of the detector, which might influence the count rate performance of the system.

Fig. 6(a) and (b) show the spatial resolution in terms of FWHM and FWTM, respectively, calculated as an average over the entire detector surface as a function of the number of reference events per irradiation position  $n_{ref}$ . Due to the somewhat small dimensions of the detector, the influence of the edges is large and, thus, the relative differences between the

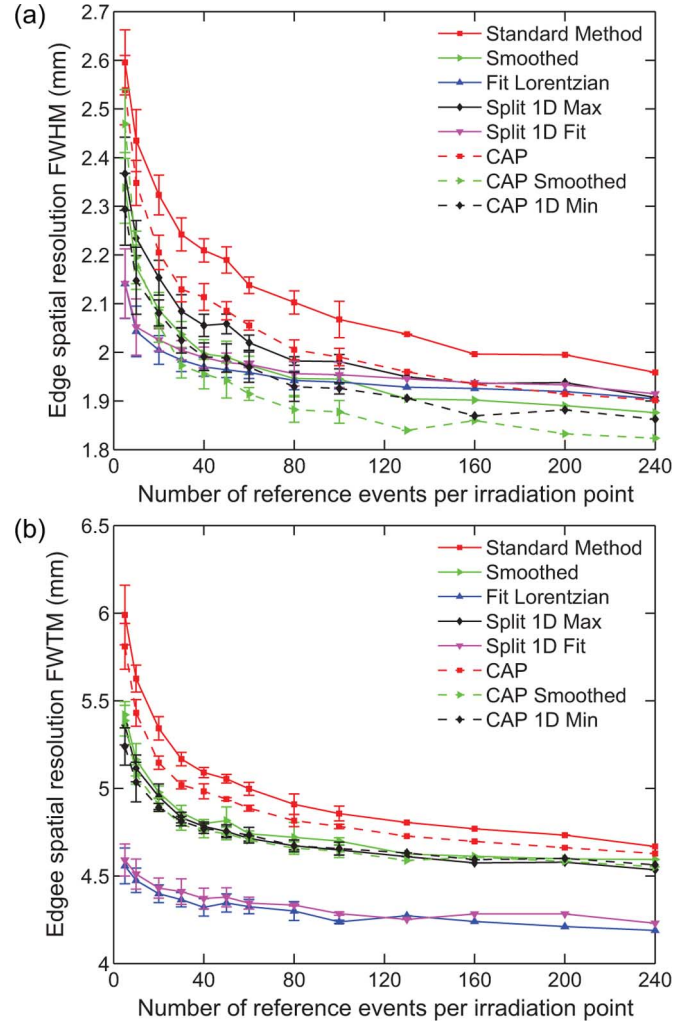


Fig. 5. Spatial resolution in terms of (a) FWHM and (b) FWTM calculated as an average over the edges of the detector surface as a function of  $n_{ref}$  for all methods investigated using a constant irradiation grid spacing of 0.25 mm.

methods are comparable to the case of the detector edges. It is shown that all alternative methods yield a better spatial resolution, FWHM as well as FWTM, than the standard method. This improvement varies from  $\sim 10\%$  to  $\sim 25\%$  depending on  $n_{ref}$ .

More specifically, when comparing the CAP methods to their equivalent 'normal' methods, i.e., standard method vs. CAP, smoothed vs. CAP smoothed, and split 1D max vs. CAP 1D min, the CAP versions perform better. Apparently, the CAP methods make use of the information contained in the reference events more effectively in the interaction position estimation.

Furthermore, the CAP smooth method outperforms all other methods in terms of FWHM, whereas the two fitting methods give better results than the others in terms of FWTM. These two fitting methods yield an almost constant value for the spatial resolution as a function of  $n_{ref}$ , i.e.,  $\sim 1.85$  mm for FWHM and  $\sim 4.25$  mm for FWTM.

A noteworthy result is the fact that the 1D methods perform at least as well and in most cases even better than the corresponding 2D method. This could be explained by the fact that,

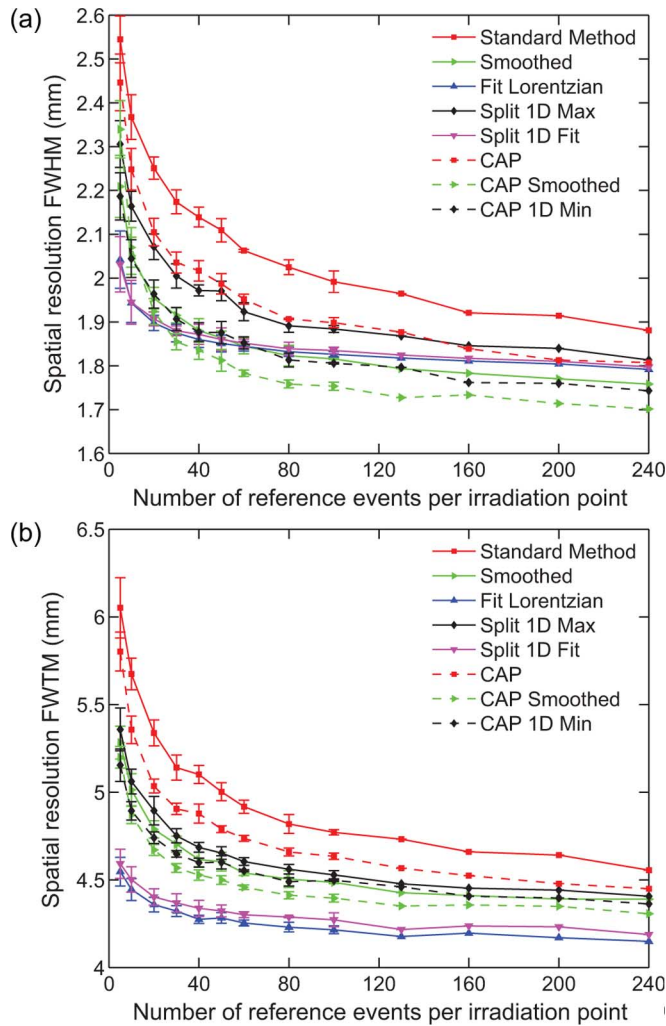


Fig. 6. Spatial resolution in terms of (a) FWHM and (b) FWTM calculated as an average over the entire detector surface as a function of  $n_{\text{ref}}$  for all methods investigated using a constant irradiation grid spacing of 0.25 mm.

given a total number of reference events, there is more reference data per 1D coordinate.

Fig. 7(a) and (b) show the spatial resolution in terms of FWHM and FWTM, respectively, calculated as an average over the entire detector surface, as a function of the total number of reference events  $n_{\text{tot}}$ . Each value of  $n_{\text{tot}}$  in general allows different combinations of  $n_{\text{ref}}$  and  $n_{\text{pos}}$  (see (1)), each yielding different values for the spatial resolution. This should be taken into account when reducing the amount of reference data to speed up calibration measurements. However, to provide a clear view of the spatial resolution in Fig. 7(a) and (b),  $n_{\text{tot}}$  was binned with logarithmically increasing bin size and for each bin center only the best spatial resolution is displayed.

The figures show that all alternative methods give a better spatial resolution than the standard method at practically all  $n_{\text{tot}}$ , in terms of FWHM as well as FWTM. Moreover, the CAP smooth method, the CAP 1D Min method, as well as the fitting methods, require  $\sim 10$  to  $\sim 20$  times less reference events than the standard method to obtain the same spatial resolution. Furthermore, the two smoothing methods yield a spatial resolution in terms of FWHM that is only slightly deteriorated at

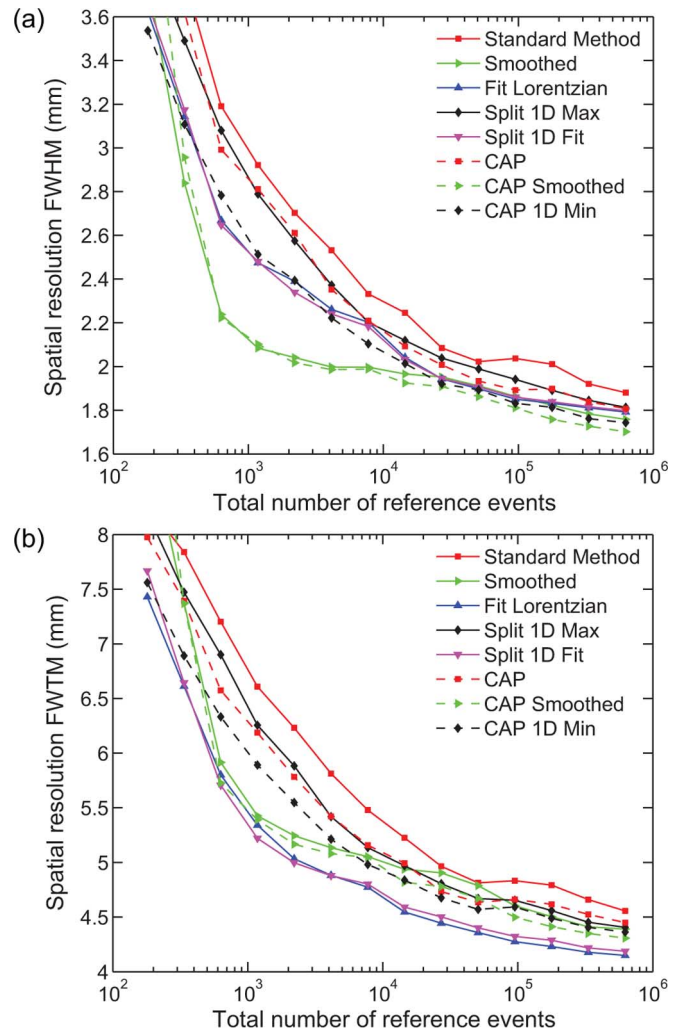


Fig. 7. Spatial resolution in terms of (a) FWHM and (b) FWTM calculated for the entire detector surface a function of  $n_{\text{tot}}$  for all methods investigated. As explained in the text, both the irradiation grid spacing and the number of reference events per irradiation point were varied.

$\sim 200$  times less reference events, i.e.,  $\sim 2.0$  mm compared to  $\sim 1.9$  mm.

If the latter result is multiplied by the calibration time reduction that can be obtained by calibrating at a single angle of incidence and/or by using a line source (see Section II), a single detector might be calibrated within minutes. This would enable the calibration of all detectors in a PET system within a reasonable amount of time. Thus, using the improvements proposed in this work, the calibration may no longer be a limiting factor for the application of monolithic scintillator detectors in PET scanners.

This result furthermore implies that the exemplary computation time, given in Section I for the calculation of the positions of interaction for a PET scan of several hundreds of millions of coincidences, might be reduced from to order of years to days. Moreover, it is expected that optimization of the implementation of the position estimation algorithm, parallelization of processes on multiple CPUs, and data preprocessing, may further reduce the computation time by several orders of magnitude. This then would decrease the computation time to the order of

minutes, bringing the  $k$ -NN method within reach for practical use in PET scanners.

Finally, it is noted that when a calibration measurement with a reduced total number of reference data  $n_{\text{tot}}$  is performed, it should be considered that there may be a combination of the number of reference events per irradiation position  $n_{\text{ref}}$  and the number of irradiation positions  $n_{\text{pos}}$  that provides optimum spatial resolution. The most favorable combination of  $n_{\text{ref}}$  and  $n_{\text{pos}}$  differs per  $k$ -NN method and, therefore, should be obtained empirically for each detector and for each implementation of the  $k$ -NN method separately.

### B. Bias Sensitivity

Fig. 8(a), (b), and (c) show the bias sensitivity  $S$  as defined in Section V-B calculated as an average over the entire detector surface, the central part, and the edges, respectively, as a function of  $n_{\text{ref}}$  where the irradiation grid spacing was kept constant at 0.25 mm. Considerable differences between the methods are observed when considering the total detector surface. However, it appears that in the detector center the bias sensitivity is small and roughly equal for all methods, in contrast to the edges of the detector. In the latter case the substantial bias sensitivity for the smoothing methods could be explained by the fact that the averaging kernel becomes smaller as well as asymmetrical close to the edges. For the fitting methods the larger bias sensitivity could be attributed to the fact that for interaction positions closer to the edge the shape of the 2D  $k$ -NN-histogram might be different from the rest of the detector (see Sections IV-A and IV-B). Furthermore, close to the edges the PSF is cut off and due to this loss of symmetry the fitting may introduce a bias, since the actual shape of the histogram is not necessarily a Lorentzian.

## VII. CONCLUSIONS

Various methods for improving the standard  $k$ -nearest neighbor method used to determine the gamma photon  $(x, y)$ -position of interaction in monolithic scintillator detectors for PET have been investigated.

For a given number of reference events,  $\sim 10\%$  to  $\sim 25\%$  better spatial resolution can be obtained by utilizing the information contained in the full set of nearest neighbors instead of only the one occurring most frequently.

Additionally, several of the alternative methods investigated yield a spatial resolution that is only slightly deteriorated, i.e.,  $\sim 2.0$  mm FWHM compared to  $\sim 1.9$  mm FWHM, when using  $\sim 200$  times less reference events. Using these methods, the detector could be calibrated  $\sim 200$  times faster, but also the position estimation using the  $k$ -NN method may be accelerated with up to the same factor.

Moreover, it was shown that the  $k$ -NN method can make use of reference data corresponding to a line of irradiation points instead of singular points. The methods equivalent to calibrating with a line source yielded at least as good results as the standard method, while allowing for much faster and easier collection of the reference data.

It appeared that, compared to the standard method, the relative bias sensitivity of the improved methods was larger at the

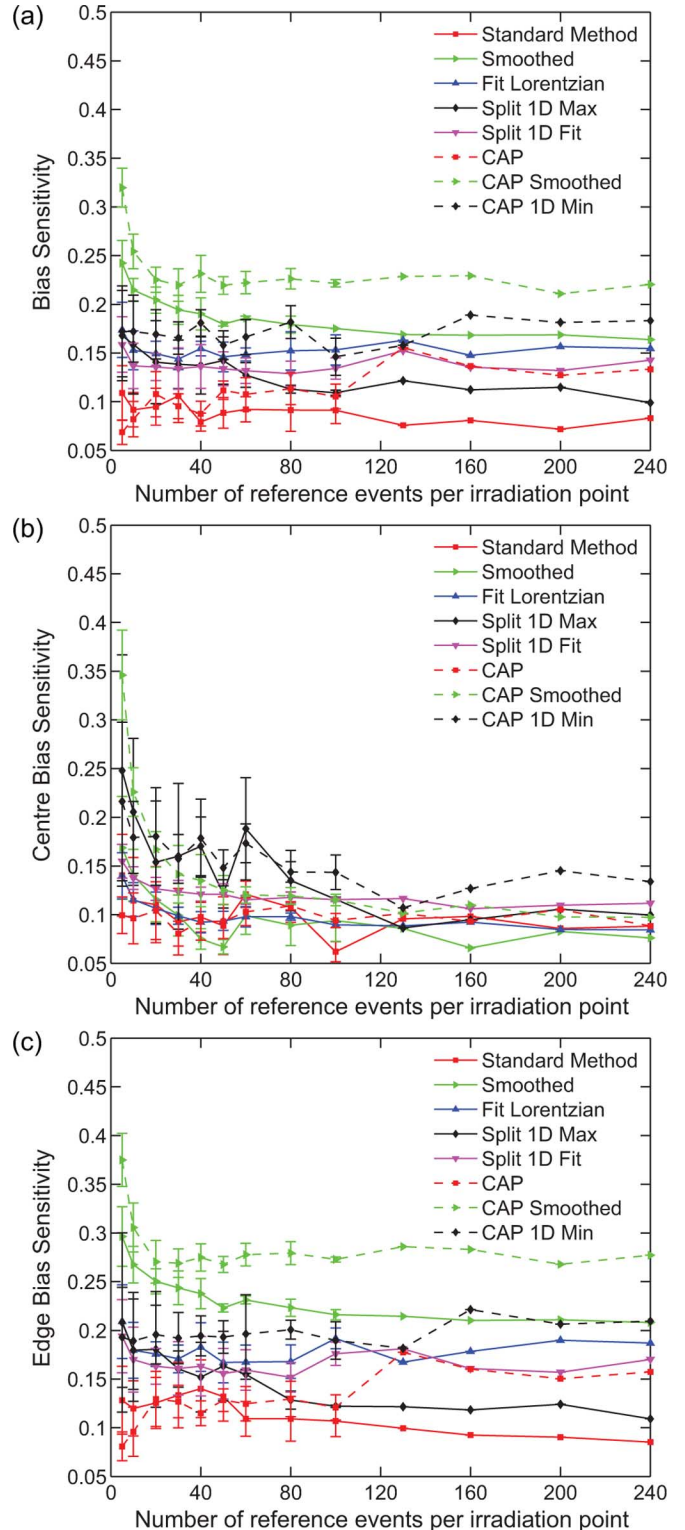


Fig. 8. Bias sensitivity  $S$  as defined in Section V-B calculated as an average over (a) the entire detector surface, (b) the central part of the detector surface, and (c) the edges of the detector surface, as a function of  $n_{\text{ref}}$  for all methods investigated using a constant irradiation grid spacing of 0.25 mm.

detector edges. This should be taken into account when modeling the detector spatial response, e.g., for image reconstruction purposes.

This work focused on several improvements of methodology, which may enable use of monolithic scintillators and/or the  $k$ -NN method in PET systems. However, the practical realization of a calibration method as well as a position estimation algorithm for monolithic scintillator detectors in a PET system will require further research as the details of the actual implementation have a strong influence on the calibration and computation times. All aspects of the implementation should be optimized taking into account e.g., the calibration source(s), collimator(s), and data preprocessing methods. In the implementation of the position estimation algorithm, aspects such as code efficiency, parallelization of processes, and data handling, will need to be studied.

It is, however, to be emphasized that the proposed improvements are multiplicative with the gains that can be obtained through implementation efficiency. Thus, the present results form an essential contribution to the development of methods that allow accelerated and facilitated calibration as well as position estimation in monolithic scintillator detectors, while maintaining their good performance.

Finally, we conclude that, using the improvements proposed in this work, the high spatial resolution obtainable with the  $k$ -NN method may come within practical reach and, furthermore, the calibration may no longer be a limiting factor for the application of monolithic scintillator detectors in PET scanners.

#### REFERENCES

- [1] P. Bruyndonckx *et al.*, "Neural network-based position estimators for PET detectors using monolithic LSO blocks," *IEEE Trans. Nucl. Sci.*, vol. 51, no. 5, pp. 2520–2525, Oct. 2004.
- [2] M. C. Maas *et al.*, "Experimental characterization of monolithic-crystal small animal PET detectors read out by APD arrays," *IEEE Trans. Nucl. Sci.*, vol. 53, no. 3, pp. 1071–1077, Jun. 2006.
- [3] P. Bruyndonckx, C. Lemaitre, D. R. Schaart, D. J. van der Laan, M. C. Maas, M. Krieguer, O. Devroede, and S. Tavernier, "Investigation of an in situ position calibration method for continuous crystal-based PET detectors," *Nucl. Instrum. Methods Phys. Res. A*, vol. 571, pp. 304–307, 2007.
- [4] T. Ling, T. K. Lewellen, and R. S. Miyaoka, "Depth of interaction decoding of a continuous crystal detector module," *Phys. Med. Biol.*, vol. 52, pp. 2213–2228, 2007.
- [5] S. K. Moore, W. C. J. Hunter, L. R. Furenlid, and H. H. Barrett, "Maximum-likelihood estimation of 3D event position in monolithic scintillation crystals: Experimental results," in *Nuclear Science Symp. Conf. Rec.*, 2007, pp. 3691–3694.
- [6] M. C. Maas *et al.*, "Monolithic scintillator PET detectors with intrinsic depth-of-interaction correction," *Phys. Med. Biol.*, vol. 54, pp. 1893–1908, 2009.
- [7] J. Benlloch *et al.*, "Design and calibration of a small animal PET scanner based on continuous LYSO crystals and PSPMTs," in *IEEE Nuclear Science Symp. Conf. Rec. 2006, NSS '06*, San Diego, CA, pp. 2328–2332, (M07-6).
- [8] D. J. van der Laan *et al.*, "Simulated performance of a small-animal PET scanner based on monolithic scintillation detectors," *Nucl. Instrum. Methods Phys. Res. A*, vol. 571, pp. 227–230, 2007.
- [9] D. R. Schaart *et al.*, "A novel, SiPM-array-based, monolithic scintillator detector for PET," *Phys. Med. Biol.*, vol. 54, pp. 3501–3512, 2009.
- [10] H. T. van Dam *et al.*, "A practical method for depth of interaction determination in monolithic scintillator PET detectors," *Phys. Med. Biol.*, 2011, accepted for publication.
- [11] E. Fix and J. L. Hodges, *Discriminatory Analysis, Nonparametric Discrimination: Consistency Properties* USAF School of Aviation Medicine, Randolph Field, TX, Technical Report 4, 1951.
- [12] T. Bailey and A. K. Jain, "A note on distance-weighted  $k$ -Nearest neighbor rules," *IEEE Trans. Syst., Man, Cybern.*, vol. 8, no. 4, pp. 311–313, Apr. 1978.
- [13] T. M. Cover and P. E. Hart, "Nearest neighbor pattern classification," *IEEE Trans. Inf. Theory*, vol. 13, no. 1, pp. 21–27, 1967.
- [14] T. Denoeux, "A  $k$ -Nearest-Neighbor classification rule based on Dempster-Shafer theory," *IEEE Trans. Syst., Man, Cybern.*, vol. 25, no. 5, pp. 804–813, May 1995.
- [15] S. A. Dudani, "The distance-Weighted  $k$ -Nearest-Neighbor rule," *IEEE Trans. Syst., Man, Cybern.*, vol. 6, pp. 325–327, 1976.
- [16] J. E. Macleod, A. Luk, and D. M. Titterton, "A re-examination of the distance-weighted  $k$ -nearest neighbor classification rule," *IEEE Trans. Syst. Man, Cybern.*, vol. 17, no. 4, pp. 689–696, 1987.
- [17] B. V. Dasarthy, "Nosing around the neighborhood: A new system structure and classification rule for recognition in partially exposed environments," *IEEE Trans. Pattern Anal. Machine Intell.*, vol. PAMI-2, no. 1, pp. 67–71, 1980.
- [18] J. M. Keller, M. R. Gray, and J. A. Givens, "A fuzzy  $k$ -NN neighbor algorithm," *IEEE Trans. Syst. Man, Cybern.*, vol. 15, no. 4, pp. 580–585, 1985.
- [19] S. Hotta, S. Kiyasu, and S. Miyahara, "Pattern recognition using average patterns of categorical  $k$ -Nearest neighbors," in *Proc. IEEE 17th Int. Conf. Pattern Recognition (ICPR '04)*, 2004, vol. 4, pp. 412–415.
- [20] S. Seifert *et al.*, "A high bandwidth preamplifier for SiPM-based TOF PET scintillation detectors," in *Nuclear Science Symp. Conf. Rec.*, 2008, pp. 1616–1619.
- [21] M. C. Maas *et al.*, "Model of the point spread function of monolithic scintillator PET detectors for perpendicular incidence," *Med. Phys.*, vol. 37, no. 4, pp. 1904–1913, Apr. 2010.